Supplemental Figure 1

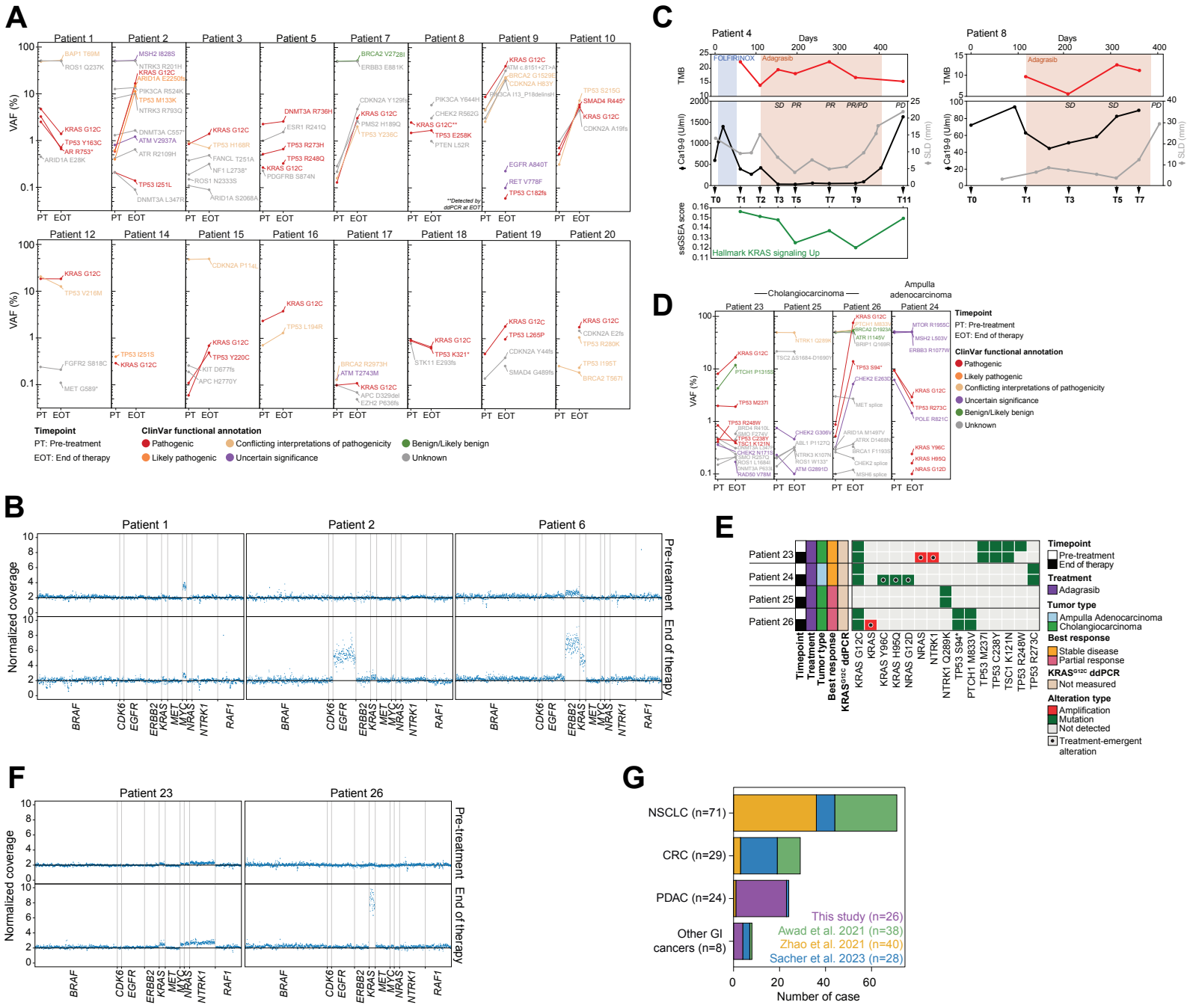

Supplemental Figure 1: Acquired resistance to KRAS^{G12C} inhibition in PDAC and other GI cancers. (A) Variant allele frequencies (VAF) for the indicated genomic variants in pre-treatment (PT) end of therapy (EOT) ctDNA samples across patients with PDAC treated with either adagrasib monotherapy on the KRYSTAL-1 trial or sotorasib monotherapy on the CodeBreaK100 trial. Colors denote ClinVar functional annotations. **(B)** Copy number profiles from targeted sequencing panel showing amplification of drivers of resistance to adagrasib monotherapy at the end of treatment (EOT, bottom panel) in comparison to pre-treatment (top panel), in three patients with PDAC. Selected genes are labeled below. **(C)** Top: Panel depicts the longitudinal monitoring of CA19-9 levels (black lines), sum of lesion diameters (SLD, grey lines) and tumor mutational burden (TMB, red lines) during treatment with adagrasib in two patients with PDAC. Bottom: Longitudinal evolution of Hallmark KRAS activity transcriptional signature in extravesicular RNA (evRNA) during treatment with adagrasib. PR: Partial response; SD: Stable disease; PD: Progressive disease. Treatment phases are indicated for each patient according to days on therapy (top axis label), with time points (T) for each ctDNA sample indicated below. **(D)** Variant allele frequencies (VAF) for the indicated genomic variants in pre-treatment (PT) and end of therapy (EOT) ctDNA samples across three patients with cholangiocarcinoma and one with ampullary adenocarcinoma who were treated with adagrasib monotherapy on the KRYSTAL-1 trial. Colors denote ClinVar functional annotations. **(E)** Comutation plot displaying genomic amplification of putative drivers of resistance to adagrasib for patients 23-26 (cholangiocarcinoma and ampullary adenocarcinoma), along with pathogenic and likely pathogenic variants detected in baseline and EOT ctDNA samples. Best radiographic treatment response is indicated as measured by RECIST criteria. **(F)** Copy number profiles from targeted sequencing panel showing amplification of drivers of resistance to adagrasib at end of treatment (EOT, bottom panel) in comparison to baseline (top panel) in two patients with cholangiocarcinoma with selected genes noted below. **(G)** Barplot depicting the study of origin, cancer types and number of patients used to evaluate mechanisms of resistance to KRASG12C inhibition across cancer types for the analysis depicted in Figure 1D.

Supplemental Figure 2

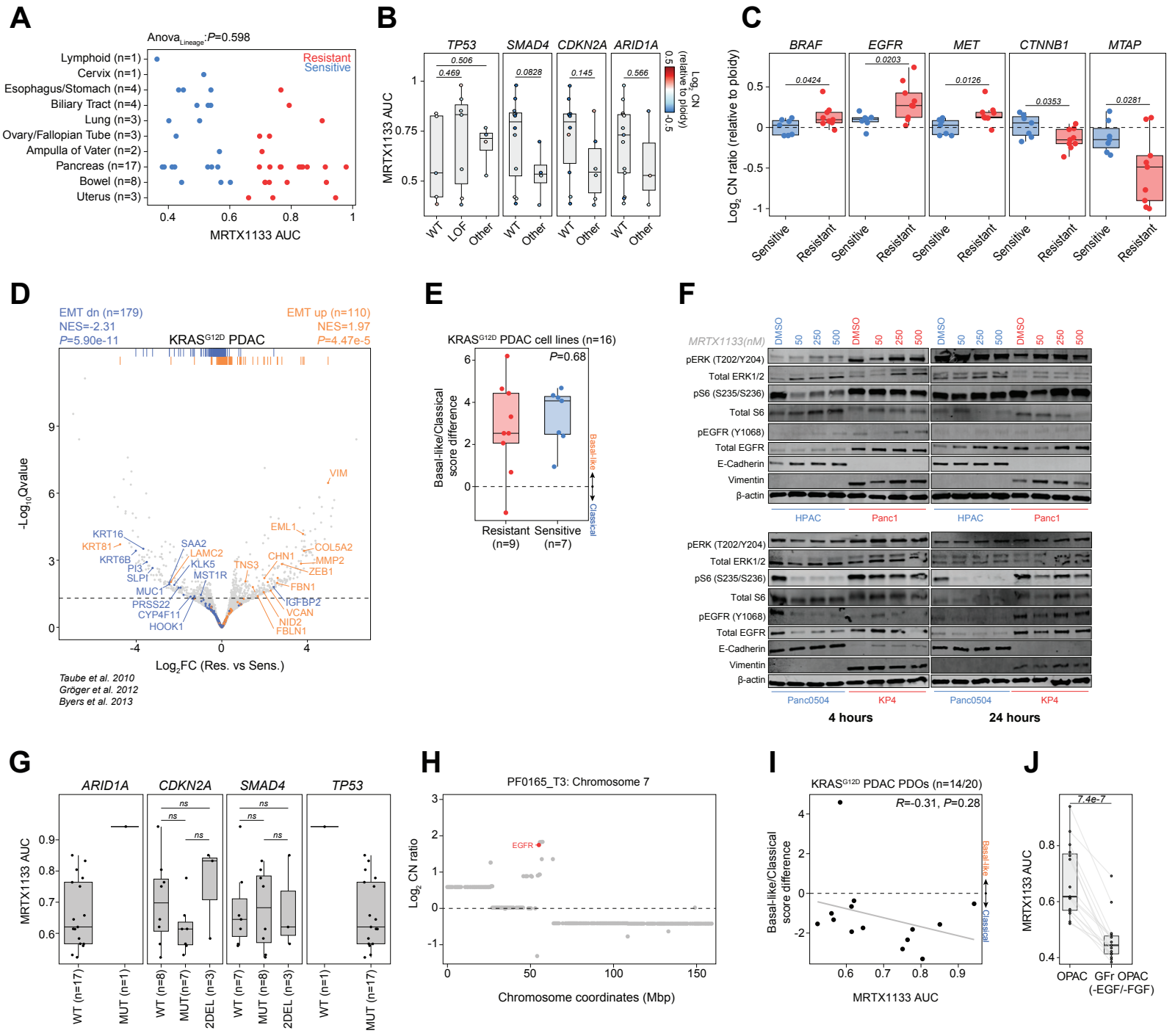

Supplemental Figure 2: MRTX1133 sensitivity across KRAS^{G12D} mutant in vitro models of PDAC. (A) Dotplot representing the area under the MRTX1133 response curve (AUC) across KRASG12D mutated cell lines in the PRISM screen. Cell lines are grouped by major lineages and colored by their relative response profile to MRTX1133. **(B)** Boxplot depicting the response to MRTX1133, displayed as AUC, across KRAS^{G12D} mutant PDAC cell lines, stratified by their mutational status for TP53, SMAD4, CDKN2A and ARID1A. Color scale indicates the Log2 ratio of copy number (relative to ploidy) for each cell line, where positive values indicate copy number elevations and negative values loss of copy number. Significance assessed by a two-sided Student's t-test. **(C**) Boxplot depicting the response to MRTX1133, displayed as AUC, across KRASG12D mutant PDAC cell lines, stratified by their copy number levels for selected genes where color denotes sensitivity and resistance (Figure 2D). The y-axis indicates the Log2 ratio copy number (relative to ploidy) for each cell line, where positive values indicate copy number elevations and negative values loss of copy number. Significance assessed by two-sided Student's t test. **(D)** Volcano plot depicting differential gene expression between MRTX1133 resistant and sensitive KRASG12D PDAC cell lines. Genes from EMT upregulation and downregulation signatures were aggregated from the 3 studies displayed and colored in orange and blue, respectively. Gene set enrichment was assessed over the unfiltered list of genes via gene set enrichment analysis (GSEA). **(E)** Boxplot depicting the subtype identity along the basal-like/classical axis (Y-axis) relative to the MRTX1133 response group (X-axis) across human *KRAS^{G12D}*-mutant cell lines (n=16) Significance determined by a two-sided Student's t-test. **(F)** Immunoblots of human KRAS^{G12D}-mutant PDAC cell lines treated with DMSO or with the indicated concentrations of MRTX1133 for 4h (left) of 24h (right). β-actin was used as protein loading control with sensitive lines labeled in blue and resistant in red. **(G)** Boxplot depicting the response to MRTX1133, displayed as AUC, across KRAS^{G12D}-mutant patient derived organoids (PDOs), stratified by their mutational and copy number status for *TP53, SMAD4, CDKN2A* and *ARID1A*. Significance assessed by a two-sided Student's t test. (**H**) Copy number profile demonstrating regions of amplification in chromosome 7 in the patient-derived organoid PF0165_T3. Genes are displayed by genomic coordinates. **(I)** Scatter plot depicting the relationship between response to MRTX1133 (AUC, X-axis) and subtype identity along the basal-like/classical axis (Y-axis) across KRAS^{G12D} PDOs (n=14). Significance determined by Pearson correlation. **(J)** Boxplots depicting the paired comparison of response to MRTX1133 (displayed as AUC) between complete organoid media (OPAC) and growth factor reduced organoid media without addition of EGF and FGF (GFr OPAC). Lines indicate paired cell lines between conditions. Significance between both conditions across all PDOs has been assessed using a two-sided Student's t test.

Supplemental Figure 3

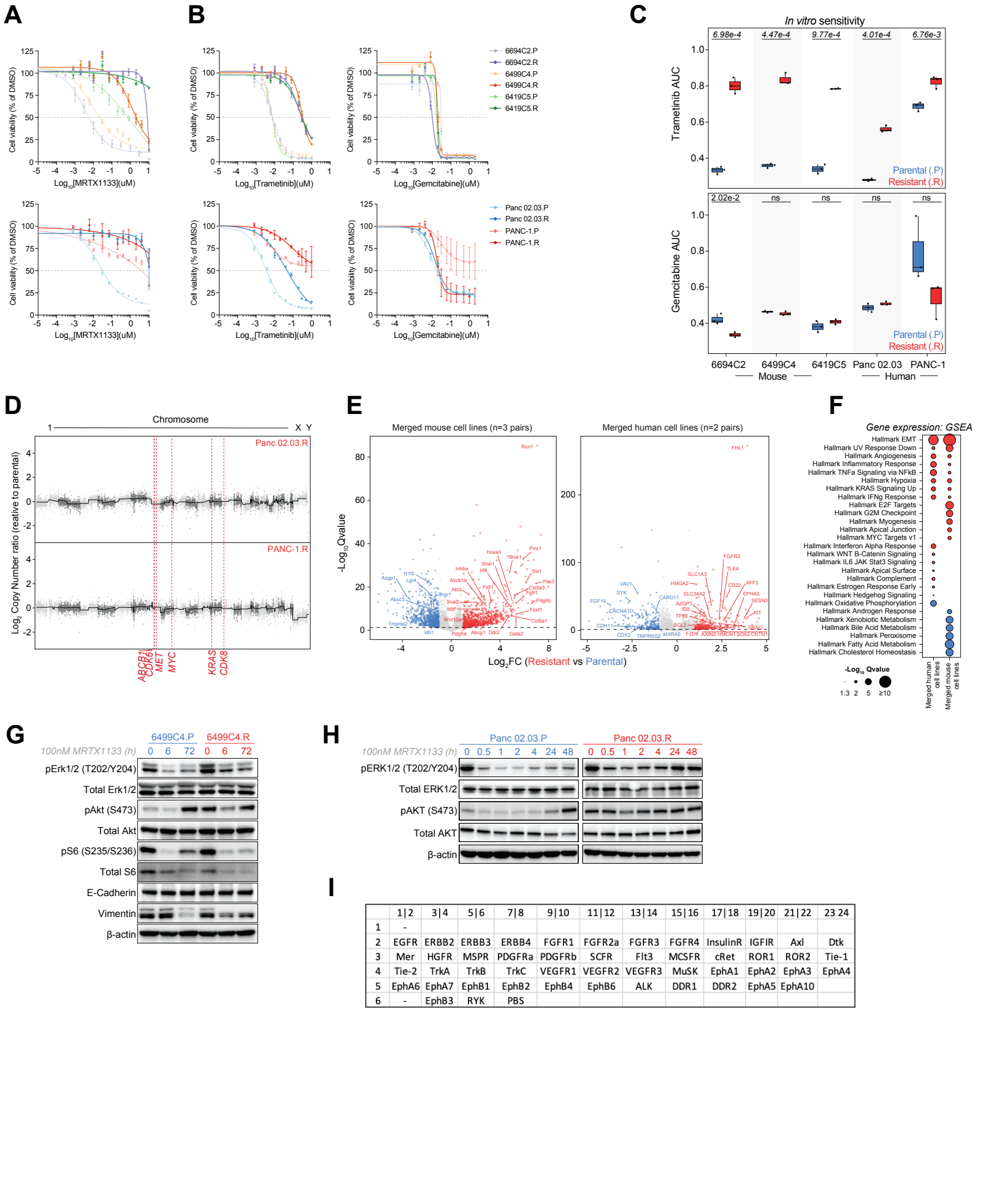

	1|2	3|4	5|6	7|8	9|10	11|12	13|14	15|16	17|18	19|20	21|22	23 24
1	-											
2	EGFR	ERBB2	ERBB3	ERBB4	FGFR1	FGFR2a	FGFR3	FGFR4	InsulinR	IGFIR	Axl	Dtk
3	Mer	HGFR	MSPR	PDGFRa	PDGFRb	SCFR	Flt3	MCSFR	cRet	ROR1	ROR2	Tie-1
4	Tie-2	TrkA	TrkB	TrkC	VEGFR1	VEGFR2	VEGFR3	MuSK	EphA1	EphA2	EphA3	EphA4
5	EphA6	EphA7	EphB1	EphB2	EphB4	EphB6	ALK	DDR1	DDR2	EphA5	EphA10	
6	-	EphB3	RYK	PBS								

Supplemental Figure 3: Isogenic models of acquired resistance to MRTX1133. (A) MRTX1133 dose response curves for a 5-day cell-titer-glo 2.0 assay with isogenic parental and resistant pairs. Legend at right with like colors representing paired lines and ".P" denoting parental, ".R" denoting resistant lines. Points are the mean ± s.e.m (n=3 biological replicates). AUC comparisons are displayed in Figure 3B. **(B)** Trametinib and Gemcitabine dose response curves for a 5-day cell-titer-glo 2.0 assay with isogenic parental and resistant pairs. Points are the mean ± s.e.m (n=3 biological replicates). **(C)** Pairwise comparison of the AUC for trametinib and gemcitabine (as displayed in Supplemental Figure 3B) between parental (blue) and derived resistant (red) cell lines. Significance determined by two-sided Student's t test (n=3 biological replicates per cell line). **(D)** Copy number profiles from whole exome sequencing of human models of acquired resistance to MRTX1133, relative to their matched parental line. Genes are organized by chromosome and genomic coordinates and amplified putative drivers of acquired resistance previously identified as amplified in human patients (Figure 1) and murine models (Figure 3) are labeled. **(E)** Volcano plot depicting aggregate differential gene expression between resistant and parental murine (left) and human (right) cell lines. Selected genes upregulated in resistant (red) or parental (blue) lines are colored and selected genes are labelled. **(F)** Hallmark gene expression sets significantly enriched by GSEA in aggregated resistant (red) compared with aggregated parental (blue) cell lines. **(G)** Immunoblots of murine isogenic parental (blue)/resistant (red) cell line pairs treated with MRTX1133 (100nM) for the indicated duration. β-actin was used as protein loading control. (H) Immunoblot of human isogenic parental (blue)/resistant (red) Panc0203 cell line treated with MRTX1133 (100nM) to the indicated time points. β-actin was used as protein loading control. **(I)** Table indicating the antibody layout for the RTK array displayed in Figure 3G.

Supplemental Figure 4

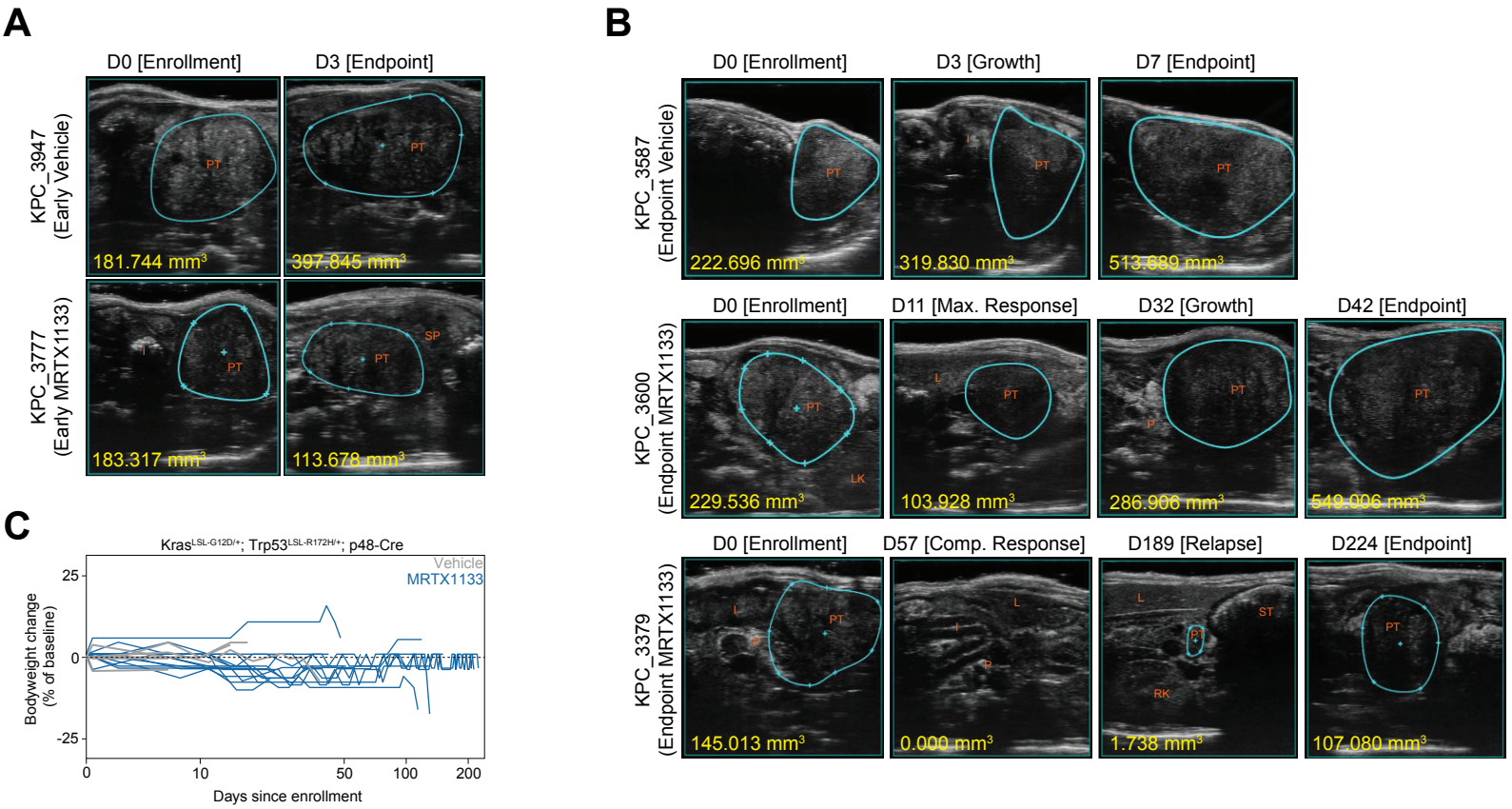

Supplemental Figure 4: In vivo treatment and tumor monitoring for the KPC PDAC mouse model. (A) Representative ultrasound images demonstrating patterns of tumor volume changes in mice sacrificed after 3 days of treatment with vehicle or MRTX1133. **(B)** Progressive imaging of specific pancreatic tumor sites in KPC mice receiving vehicle or MRTX1133 treatment until natural endpoint. Examples here demonstrate tumor growth under vehicle treatment (KPC_3587, top), partial response to MRTX1133 (KPC_3600, middle), and complete tumor clearance by MRTX1133 (KPC_3379, bottom) prior to relapse. Days and images are representative. Adjacent organs serve as indices for identifying tumor sites: Pancreatic Tumor (PT), Pancreas (P), Spleen (SP), Stomach (ST), Intestines (I), Right Kidney (RK), Left Kidney (LK), Liver (L). **(C)** Body weight of KPC mice treated with Vehicle (n=9) or MRTX1133 (n=14/15) over time until endpoint criteria were met. Body weight changes were standardized to enrollment weight. **(D)** Aggregate of clinical data and omic characterization available for all KPC mice in this study. Top bar plot indicates the best response on MRTX1133 (for endpoint MRTX1133- treated KPC mice), the largest tumor volume change during treatment (for endpoint vehicle-treated KPC mice) or the tumor volume reduction after 3 days of treatment (for early endpoint arms).

Supplemental Figure 5

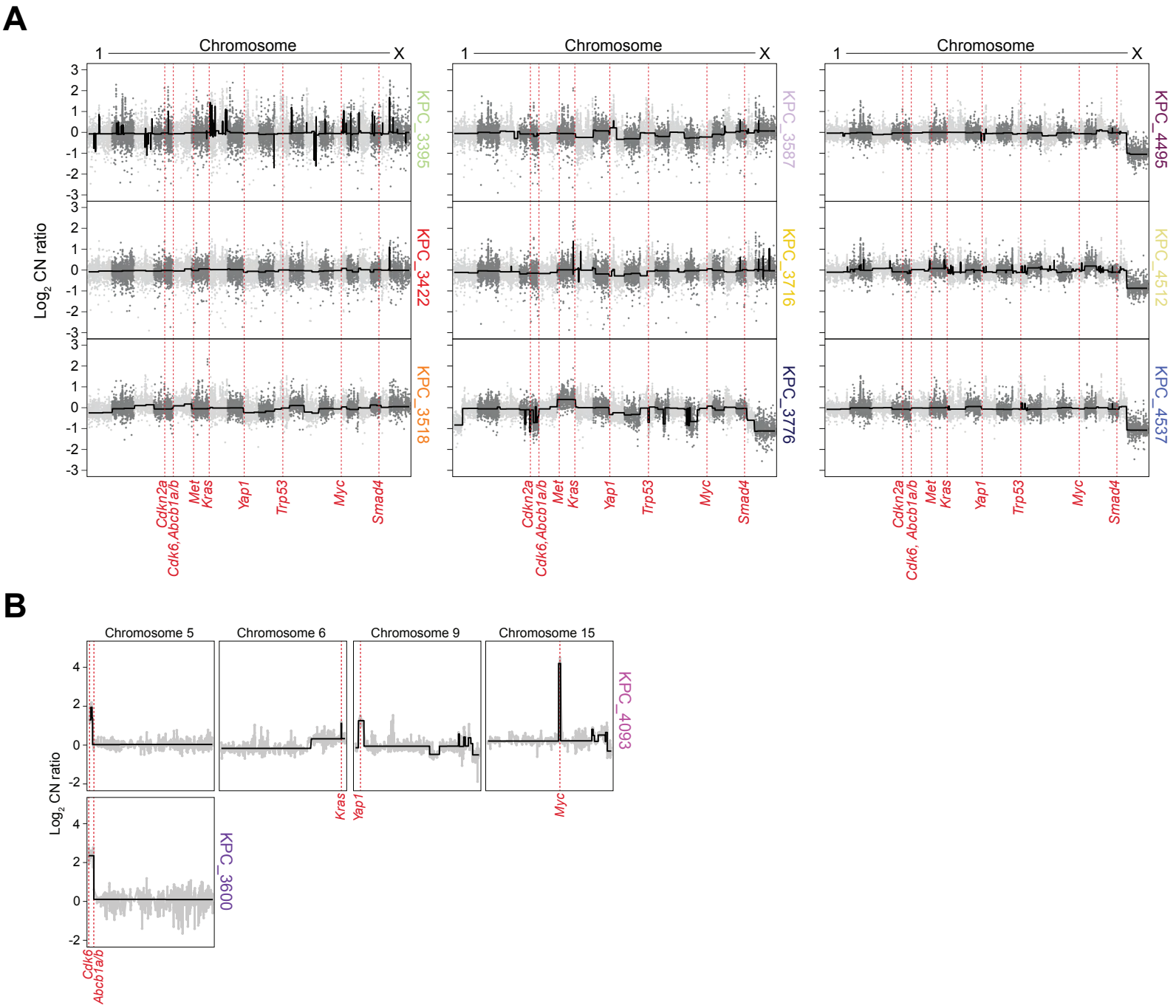

Supplemental Figure 5: Genomic characterization of KPC tumors. (A) Copy number profiles from whole exome sequencing of endpoint vehicle-treated KPC mice. Genes are organized by chromosome and genomic coordinates. Labeled are putative drivers of acquired resistance previously identified as amplified in human patients (Figure 1), murine models (Figure 3) and MRTX1133 resistant KPC mice (Figure 4). (B) Copy number profiles demonstrating regions of amplification from MRTX1133 resistant KPC tumors. Genes are displayed by genomic coordinates and segment trend is depicted by the black line. Amplified putative drivers of resistance to MRTX1133 are labeled in red, with their genomic coordinates indicated by a red dashed line.

Supplemental Figure 6

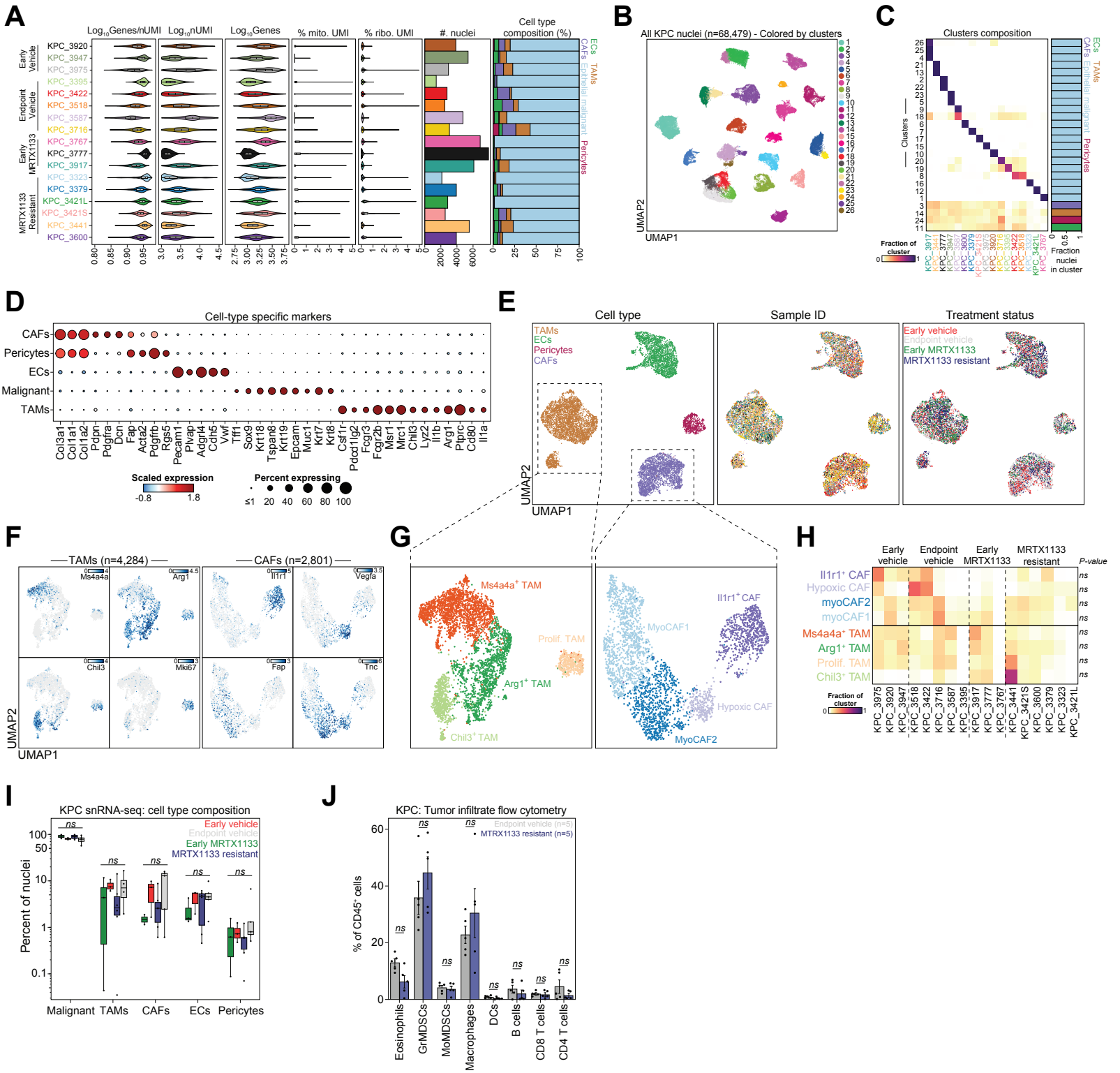

Supplemental Figure 6: snRNA-seq quality metrics and description of the tumor microenvironment. (A) Violin plots depicting the distribution of quality and sequencing metrics per nuclei in each sample from the snRNA-seq dataset after quality control (Methods). **(B)** UMAP embedding of single-nuclei from KPC PDAC tumors and colored by SNN clusters. **(C)** Distribution of single nuclei captured per sample across the identified SNN clusters in the snRNA-seq dataset. The top barplot annotation indicates the fraction of nuclei within a cluster that were classified in each cell type as displayed in Figure 4F. **(D)** Dotplot depicting the scaled average expression of cell type markers across cellular population identified in the snRNA-seq dataset. **(E)** Uniform manifold approximation and projection (UMAP) embedding of single-nuclei from KPC PDAC tumors colored by sample ID (left), cell type (center) or treatment status (right). Outlined are the three major non-malignant cell populations identified. **(F)** UMAP embeddings of TAMs (left) and CAF (right) across all KPC tumors. Each quadrant represents a cluster-specific marker and its expression level across nuclei from a TAM or CAF population. **(G)** UMAP embeddings of TAMs (left) and CAFs (right) subpopulations. **(H)** Distribution of single nuclei captured per sample across TAM and CAF subpopulations as displayed in **G**. Samples are grouped according to treatment class. Significance values are displayed on the right and were determined for each subpopulation by ANOVA on variance-stabilized nuclei proportions and were adjusted with Benjamini-Hochberg correction. **(I)** Proportion of cell types captured across samples and treatment group in the snRNA-seq dataset. Significance determined for each cell type by ANOVA on variance-stabilized nuclei proportions and were adjusted with Benjamini-Hochberg correction. **(J)** Proportion of immune populations from total tumor infiltrating immune cells captured by flow cytometry in endpoint vehicle and MRTX1133-resistant tumors. Error bars are the mean ± s.e.m (n=5 tumors per group). Significance determined by two-sided Student's t-test and adjusted with Holm-Šidák correction.

Supplemental Figure 7

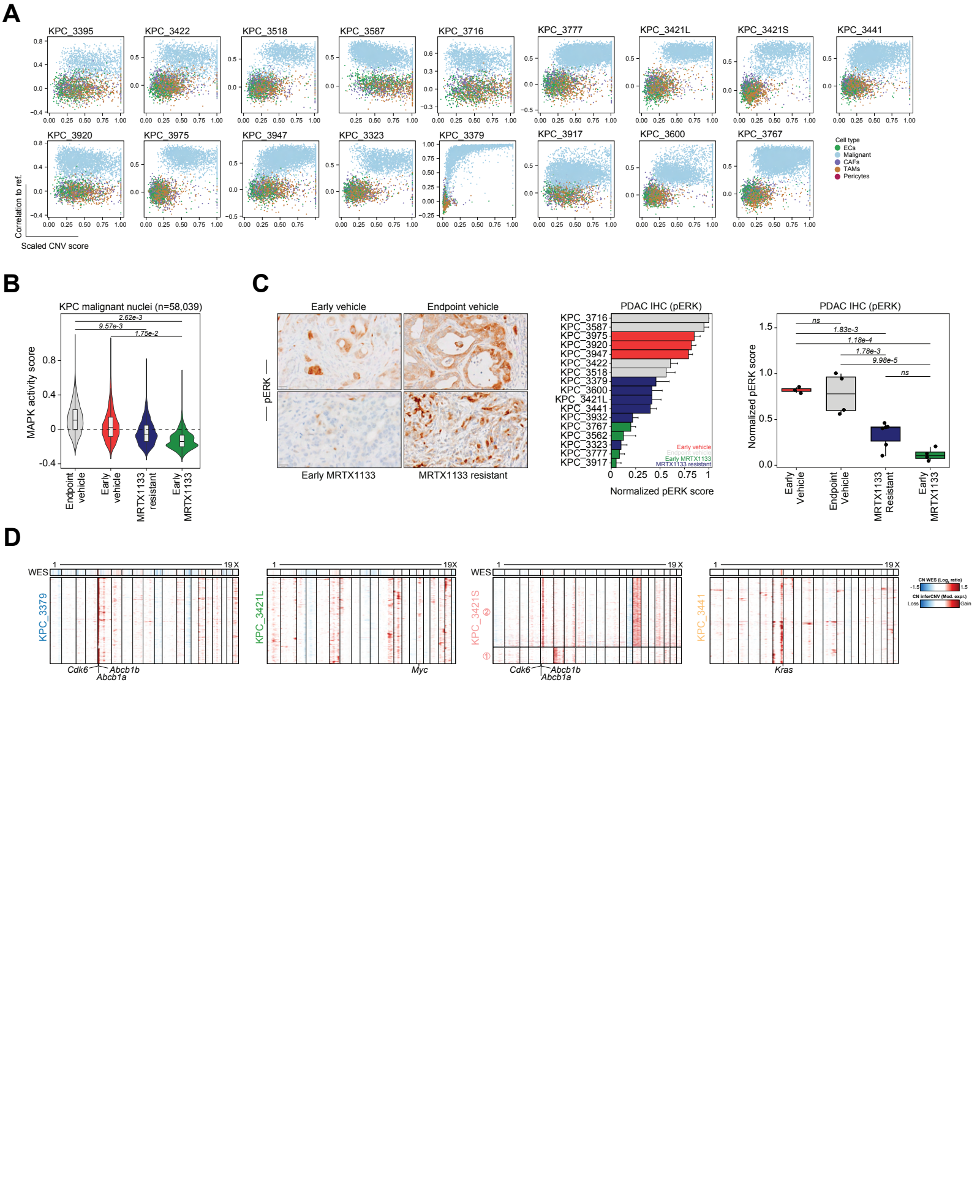

Supplemental Figure 7: Identification and characterization of malignant cell populations. **(A)** Correlation of single-nuclei copy number (CN) scores in with reference malignant nuclei (averaged top 10% altered nuclei per sample) versus scaled CN score for each nuclei used within that sample. Colors correspond to different cell types within each sample. **(B)** Violin plots depicting the distribution of Progeny's MAPK signature score across single nuclei, grouped by treatment status. Significance assessed by linear mixed effects model. **(C)** *Left*: Immunohistochemistry staining for phosphorylated ERK from representative microscopy images across treatment groups (Scale bar represents 20um). *Middle*: Sample-wise pERK normalized score from at least 2 distinct PDAC areas per tumor. Bars are mean ± s.e.m. *Right*: Boxplot depicting the treatment-group level pERK score. Comparisons and significance for inter-group differences determined by two-sided Student's t test, with p-values indicated above. **(D)** Heatmaps of single-nucleus CN profiles inferred from snRNA-seq of four MRTX1133-resistant tumors. Genes are organized by chromosome and genomic coordinates (columns). Row splits indicate major subclones identified within each tumor, if any. The top annotation bar indicates the matched genomic reference from DNA WES for the same tumor. Genomic amplifications identified by WES are labeled at the bottom. *Kras* has been labeled within the low-level gain of chromosome 6 in KPC_3441.

Supplemental Figure 8

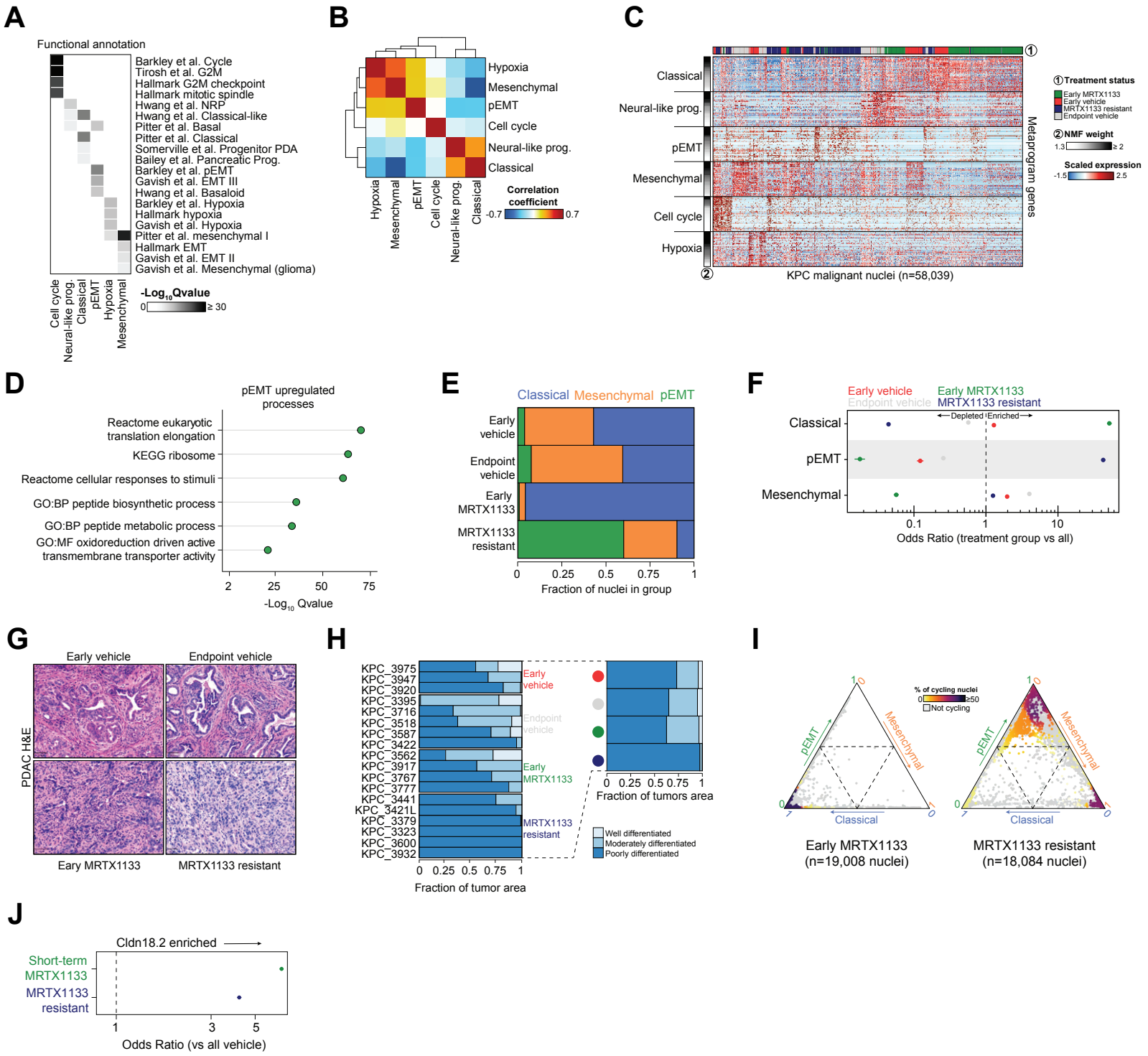

Supplemental Figure 8: Characterization of malignant metaprograms in KPC tumors. (A) Heatmap depicting the top 5 functional annotations for each metaprogram. Significance determined by hypergeometric test and adjusted with Benjamini-Hochberg correction. **(B)** Pairwise correlation analysis between metaprogram scores across malignant KPC nuclei. **(C)** Heatmap depicting the scaled expression of each metaprogram gene (rows) across the malignant single nuclei from the KPC cohort. Each major row split corresponds to a metaprogram with rows representing genes within that metaprogram, and each single column corresponds to a single nuclei. **(D)** Top enriched signatures in pEMT-specific upregulated genes (Figure 5C). Significance determined by hypergeometric test and adjusted with Benjamini-Hochberg correction. **(E)** Barplot depicting the cell state classifications by snRNA-seq across treatment groups. **(F)** Cell state-wise enrichment analysis comparing the proportion of nuclei within a cell state for each treatment group against the rest of the cohort. Odds ratios obtained from Fisher's exact test with $P<0.0001$ for all comparisons. **(G)** Representative H&E staining of KPC PDAC tumors from each treatment group. **(H)** *Left*: Sample-wise adenocarcinoma differentiation grade across KPC cohort. *Right*: Treatment group aggregated histological grade classification. **(I)** Ternary plot displaying the cell state classification probability of each nucleus across the Classical-pEMT-Mesenchymal tripartite framework, as calculated by a Markov absorption-based classifier. The coloration gradient is proportional to the fraction of cycling nuclei from a given treatment group found in the same neighborhood. **(J)** Enrichment analysis of Claudin-18.2 protein expression comparing the indicated MRTX1133 treatment groups with all vehicle-treated tumors. Odds ratios determined by Fisher's exact test. All the comparisons are significant (p-value < 0.05).

Supplemental Figure 9

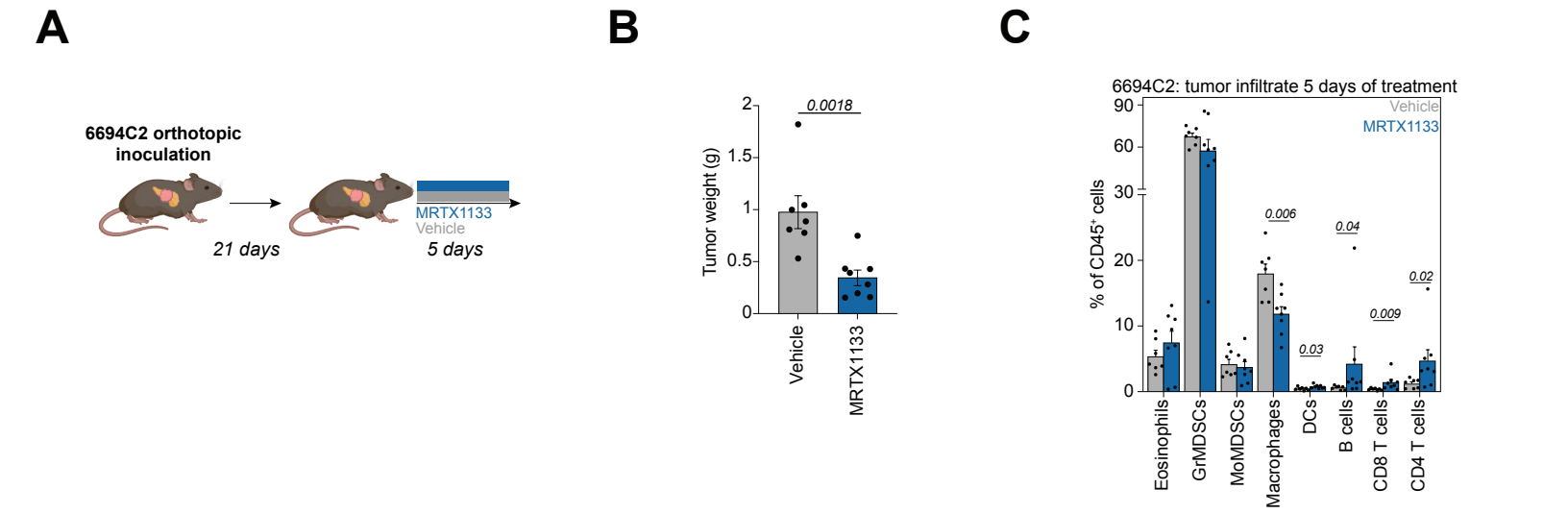

Supplemental Figure 9: Treatment with MRTX1133 induces modest changes in the immune microenvironment following tumor regression. (A) Experimental design. C57BL/6 mice were implanted orthotopically with 6694C2 tumors and treated with vehicle or MRTX1133 for 5 days starting on day 21 post-implantation. **(B)** Tumor weights after 5 days of treatment. Significance determined by a two-sided Student's t-test. **(C)** Tumors from panel A were enzymatically digested and analyzed by multispectral flow cytometry for the indicated populations. Error bars are the mean ± s.e.m (n=7-8 tumors per group). Significance determined by two-sided Wilcoxon rank sum test and adjusted with Holm-Šidák correction. Only the significant P-values are displayed (P-value ≤ 0.05).

Supplemental Figure 10

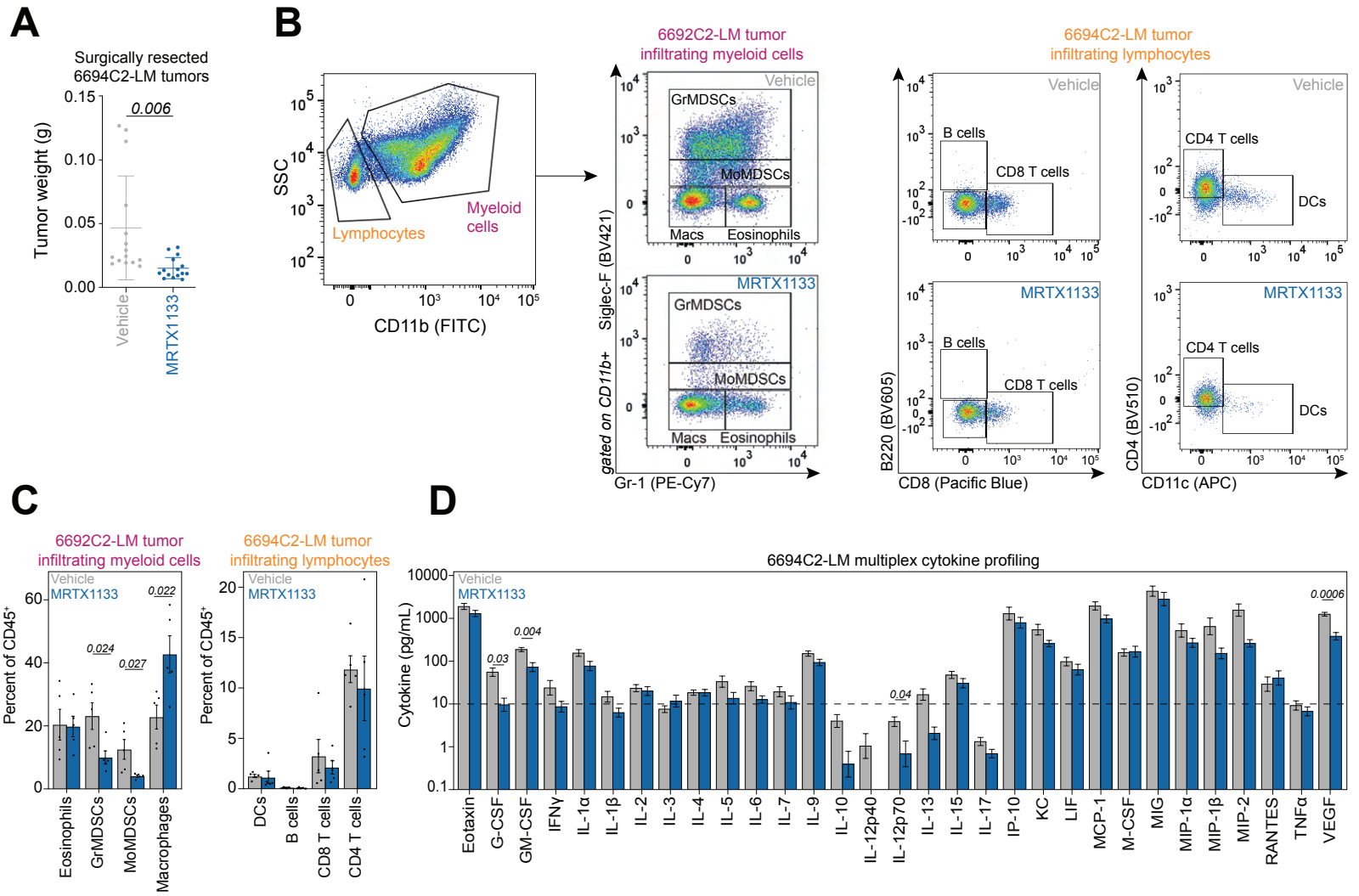

Supplemental Figure 10: Treatment of 6694C2-LM tumors with MRTX1133 reduces granulocytes but has little effect on T cells. (A) C57BL/6 mice were implanted subcutaneously with 250,000 6694C2-LM tumor cells and treated with vehicle or MRTX1133 for 5 days starting on day 6. Tumors were surgically resected, and weights are shown. **(B)** Tumors from A were enzymatically digested and analyzed by multispectral flow cytometry. Representative gating schemes for the indicated populations are shown. (Macs=macrophages; GrMDSCs=granulocytic myeloid-derived suppressor cells; MoMDSCs=monocytic myeloid-derived suppressor cells. **(C)** Quantification of myeloid (*Left*) and lymphocyte (*Right*) populations from 6694C2-LM subcutaneous tumors treated for 5 days with MRTX1133. Error bars are the mean ± s.e.m (n=5 tumors per group). Significance determined by two-sided Student's t-test and adjusted with Holm-Šidák correction. Only the significant p-values are displayed (P-value ≤ 0.05). **(D)** Protein lysates from tumors treated as in A were analyzed by cytokine bead array for the indicated cytokines. Error bars are the mean ± s.e.m (n=5 tumors per group). Significance determined by two-sided Student's t-test and adjusted with Holm-Šidák correction. Only the significant p-values are displayed (p-value ≤ 0.05).

Supplemental Figure 11

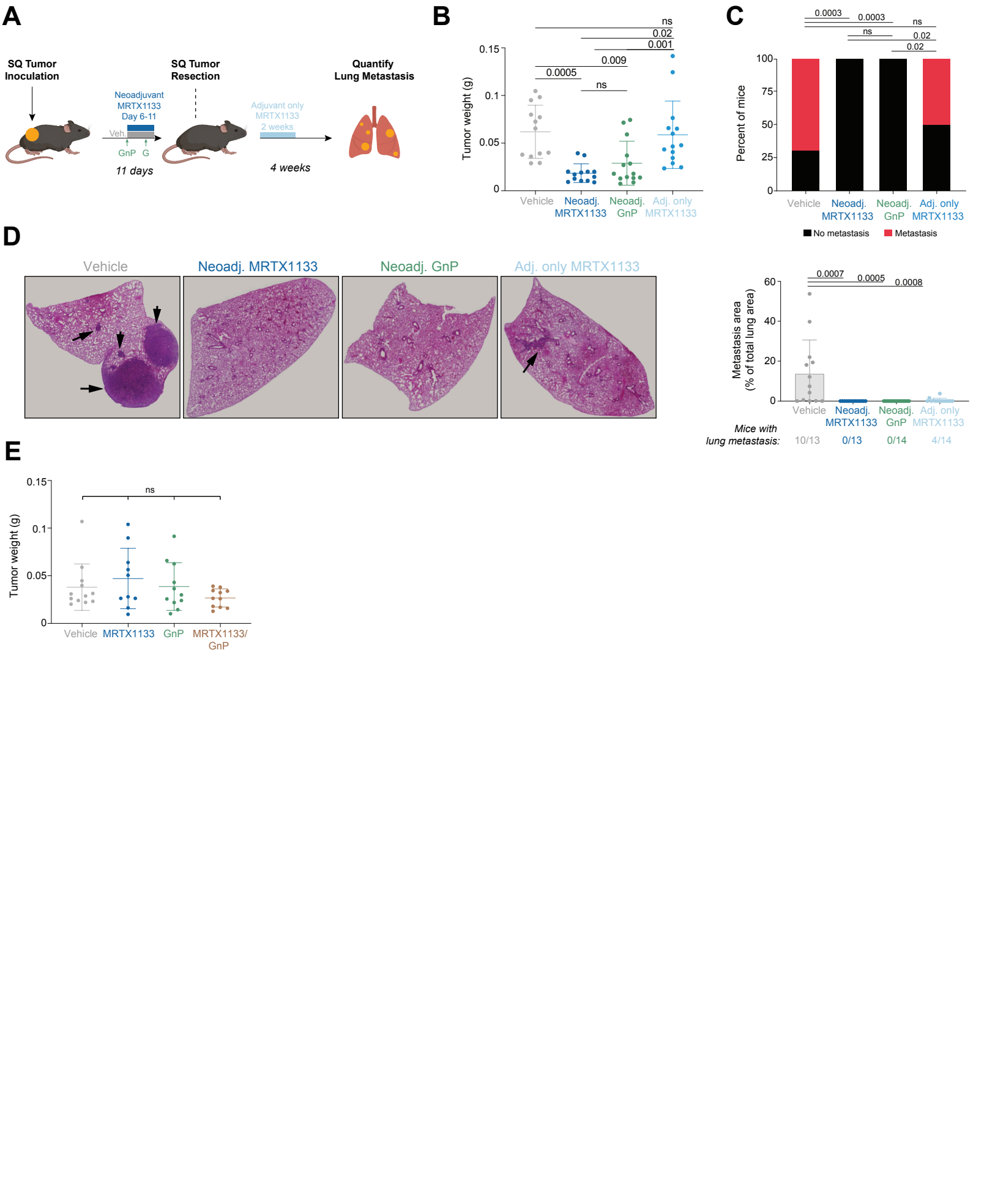

Supplemental Figure 11: Neoadjuvant and adjuvant therapy in a metastatic model of PDAC. **(A)** Model of subcutaneous tumor removal (day 11 post-inoculation) to generate metastasis using 6649C2-LM line with the treatment scheme of neoadjuvant (presurgical, days 6-11) or adjuvant (day 13-26 post-surgery) MRTX1133 compared to neoadjuvant gemcitabine/n(ab)-paclitaxel (GnP) on day 6/gemcitabine on day 8 or vehicle treatment alone. **(B)** Tumor weights at time of surgery (day 11) comparing vehicle, neoadjuvant or adjuvant MRTX1133 and neoadjuvant gemcitabine/n(ab)-paclitaxel (n=13,13,14,14). Statistics were compared using ANOVA with Tukey's multiple comparison correction with outliers 2 standard deviations away from the mean removed from the analysis. **(C)** Metastases from lungs and lymph nodes were counted at the time of harvest and the percentage of mice with metastasis at 4 weeks post-surgery (n=13,13,14,14) is shown as a barplot. Statistics were calculated using Fisher's exact test with FDR for multiple comparisons. **(D)** Representative H&E images of lungs, with black arrows indicating metastases, from the treatment groups in D at harvest 4 weeks post-surgical removal (left). Quantification of metastatic area from total lung area, one slide per animal with the total number of mice with metastasis below (n=13,13,14,14) (right). Statistics performed by ANOVA with Tukey's multiple comparison correction. **(E)** Tumor weights measured at time of surgery prior to adjuvant treatment (Figure 6E-F) for all groups. Significance determined by ANOVA followed by Tukey's HSD multiple comparisons test.